SUPPLEMENTARY INFORMATION

Probing the Magnetism of Topological End-States in 5-Armchair Graphene Nanoribbons

James Lawrence,[1,2,†] Pedro Brandimarte,[1,†] Alejandro Berdonces-Layunta, [1,2] Mohammed S. G. Mohammed, [1,2] Abhishek Grewal, [3] Christopher C. Leon, [3] Daniel Sanchez-Portal, [1,2,*] Dimas G. de Oteyza. [1,2,4,*]

[1] Donostia International Physics Center, 20018 San Sebastián, Spain

[2] Centro de Fisica de Materiales, CSIC-UPV/EHU, 20018 San Sebastián, Spain

[3] Max-Planck-Institut für Festkörperforschung, 70569 Stuttgart, Germany

[4] Ikerbasque, Basque Foundation for Science, 48013 Bilbao, Spain

[†] These authors contributed equally

[*] daniel.sanchez@ehu.eus, d_g_oteyza@ehu.eus

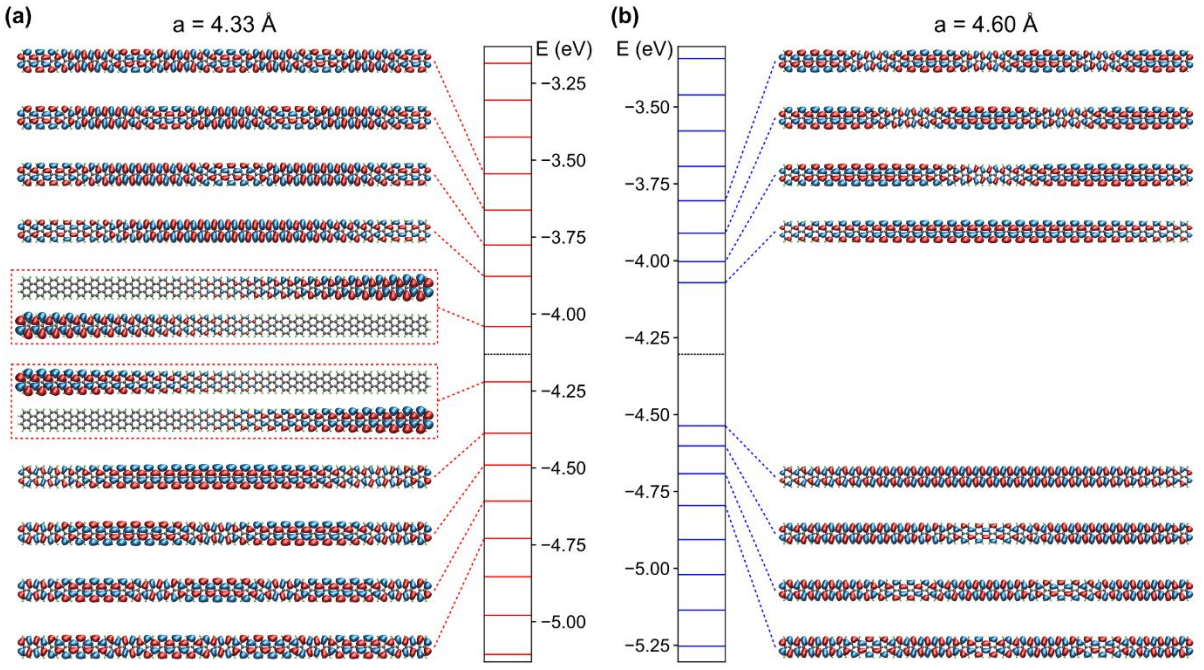

Figure S1. A comparison of gas-phase DFT calculations for the topologically (a) non-trivial and (b) trivial 30-UC 5-AGNR. The structures were built by taking the unit cell geometry optimized at a fixed lattice parameter (a = 4.33 Å for the non-trivial case and a = 4.60 Å for the trivial one, see Fig. S2), replicating it and only leaving it to further relax the hydrogen atoms. No spin-split end states can be seen on the trivial ribbon, and the orbital character of the valence and conduction band onsets are noticeably inverted from those seen in the relaxed ribbon (Fig. S2(a) and main paper Fig. 1(d)).

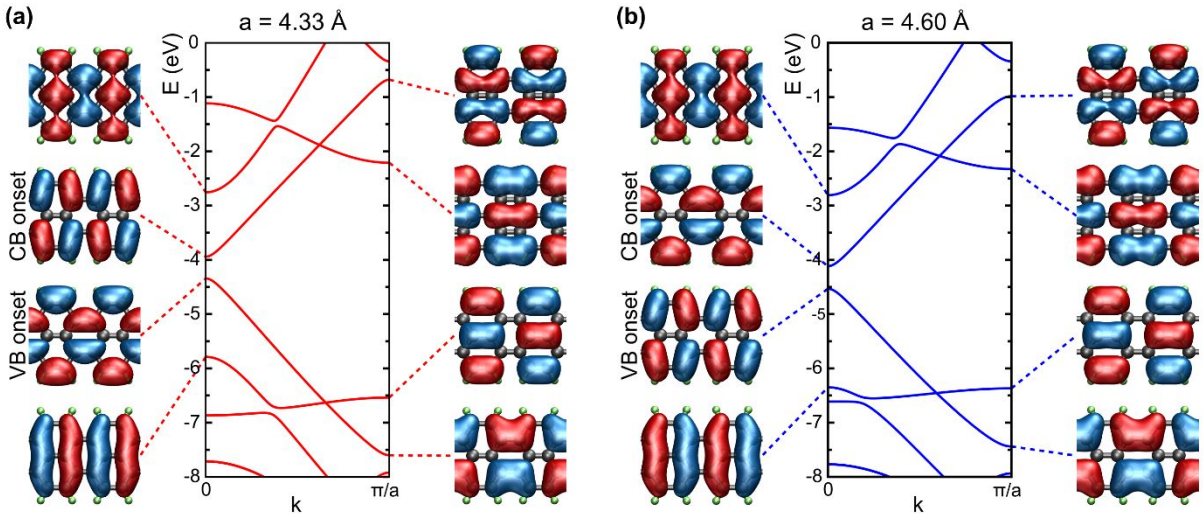

Figure S2. The calculated band structures of free-standing infinite relaxed 5-AGNRs. (a) Topologically non-trivial lowest energy configuration with lattice parameter a = 4.33 Å. (b) A topologically trivial configuration optimized at a fixed larger lattice parameter of a = 4.60 Å. The VB and CB onsets at the Γ point are exchanged when compared to the non-trivial case (a). The energies are given with respect to the vacuum level.

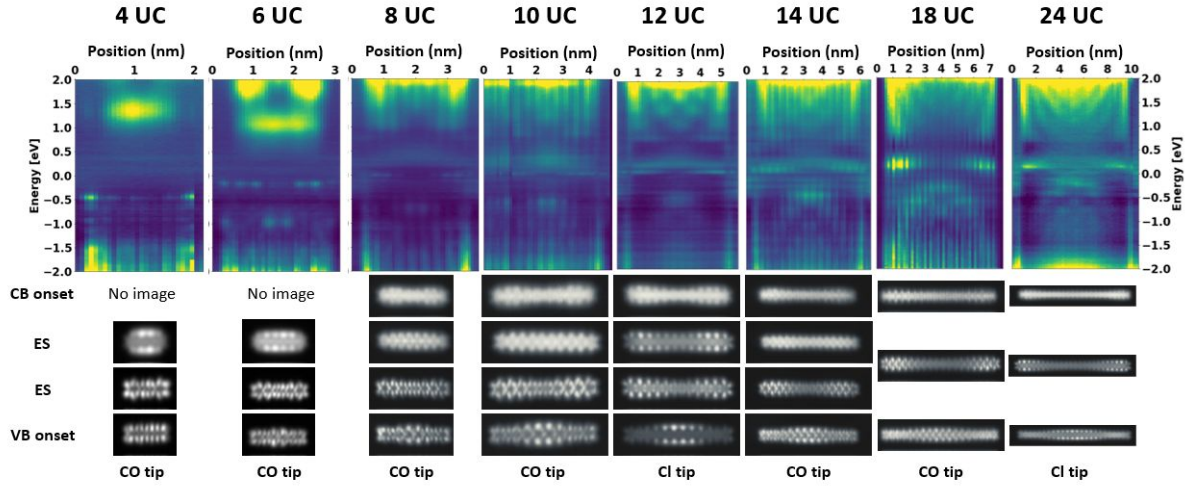

Figure S3. A series of dI/dV line scans for ribbons of increasing length, adsorbed on Au(111), accompanied by constant height dI/dV images of their CB onset, end states and VB onset (where possible). The tip used for the images is indicated below. The sharp transition seen in the 10-UC line scan is due to the ribbon moving part way through the experiment. However, all states of interest can still be seen in the region recorded before it shifted.

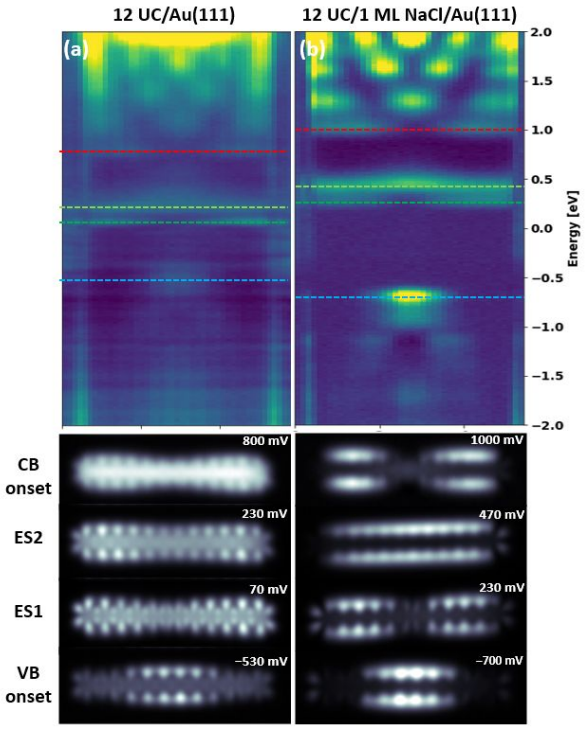

Figure S4. A comparison between dI/dV line scans and images of 12-UC ribbons on both Au(111) and 1ML NaCl islands. The states imaged in the lower half of the figure are indicated with dashed lines in the line scan. There is a clear increase in the band-gap of the ribbons when adsorbed on NaCl, as would be expected due to a reduced level of screening from the metallic substrate. However, there is also an upshift of both end-states relative to the centre of the band gap. In both cases the end states are unoccupied, that is, the ribbon is positively charged when it is adsorbed on Au(111) with or without the NaCl buffer layer.

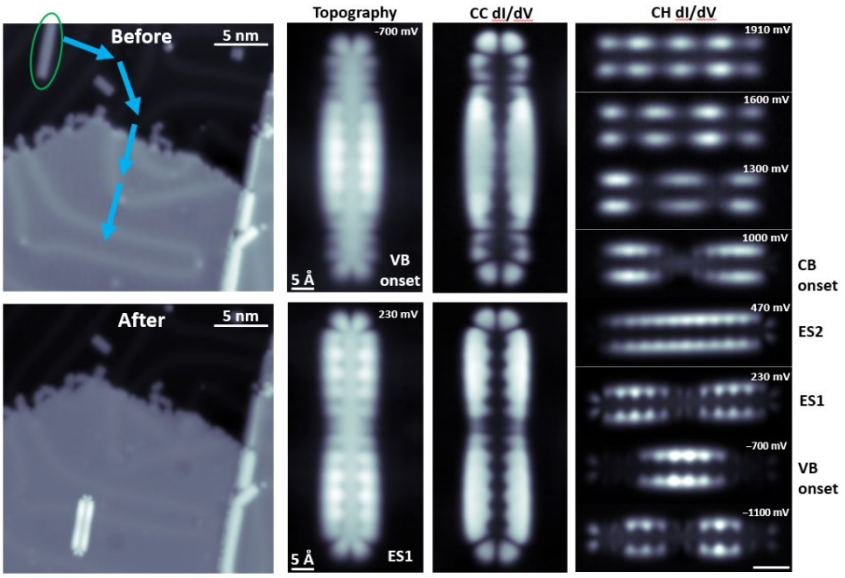

Figure S5. The manipulation and imaging of a 12-UC 5-AGNR onto a 1ML NaCl island. After making contact with the end of the ribbon with the STM tip, it was dragged along the path indicated by the blue arrows, and then lifted/dragged onto the NaCl island. Various dI/dV images of the same ribbon

are shown to the right, with both constant current (CC) and constant height (CH) images shown. The confinement effects on the electronic states of the conduction band can be much more clearly seen here, with an increasing number of nodes observed at higher bias voltages. The scale bar of the images on the right-hand side is 1 nm, and the images were recorded with a Cl-functionalized tip.

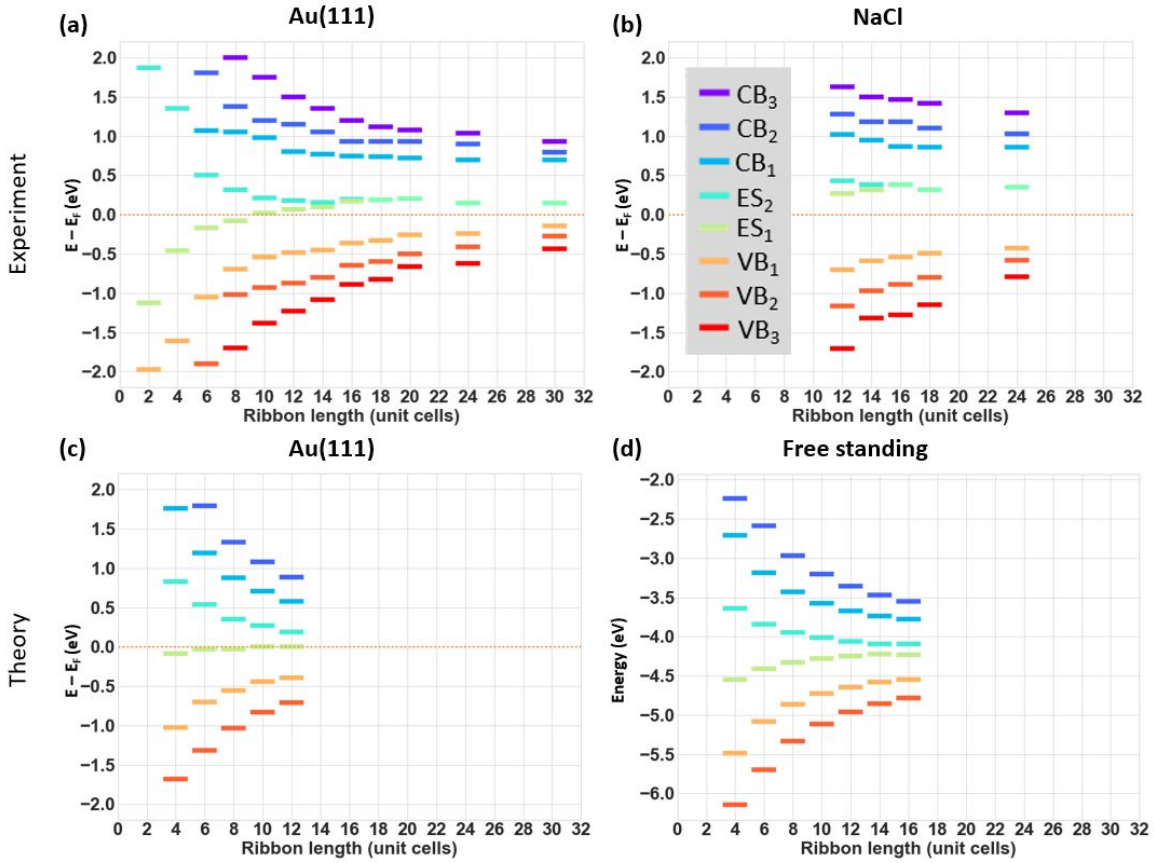

Figure S6. Energies for the lowest energy quantization states related to valence and conduction band, as well as for the in-gap end states as a function of the GNR length on Au(111) (a) and on a NaCl monolayer (b) (referred to E_F, marked with an orange dashed line at E=0). The energies of those same states from calculations on Au(111)-supported and free-standing GNRs are displayed in (c) and (d), respectively (referred to the Fermi level marked by an orange dashed line in (c) and with respect to the vacuum energy in (d)). Comparison of the data on Au(111) and NaCl/Au(111) clearly show the effect of the reduced screening (a larger apparent bandgap) on NaCl for all lengths. Beyond the different band gap values on either substrate, both datasets display a similar strong length dependence that only tends to saturation for the longest measured ribbons (beyond 20 unit cells). A comparable length dependence is observed in our calculations for both Au(111)-supported and free standing GNRs. Notice, however, that these DFT calculations do not account for all effects associated with the different screening by the different substrates, such as the energy renormalization due to the long range image potential. In addition, both on Au(111) and NaCl/Au(111) the GNRs get charged by electron donation to the high workfunction substrate for ribbons above a certain length threshold (8-10 UC on Au(111)). This is again confirmed by DFT calculations, which show a similar length threshold (10 UC) at which the GNRs become charged on Au(111). The hybridization with the Au(111) substrate provides the ribbon's levels with a finite width and in some cases makes their identification harder. However, a detailed comparison of the projected density of states on the ribbon with the energy

spectra from free-standing ribbons allows for an unambiguous identification of the levels in the DFT calculations.

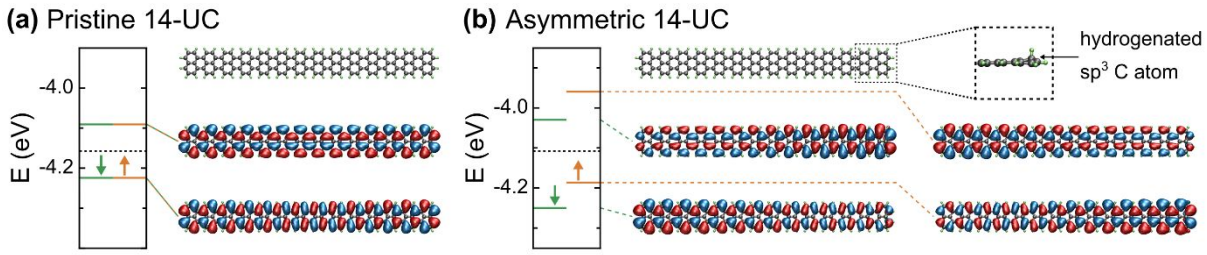

Figure S7. (a) Structure of a pristine 14-UC 5-AGNR and its associated closed-shell end state orbitals. (b) Structure of an asymmetric 14-UC 5-GNR with a hydrogenated C atom on one end and its associated open-shell end state orbitals. Orange and green lines indicate opposite spin.

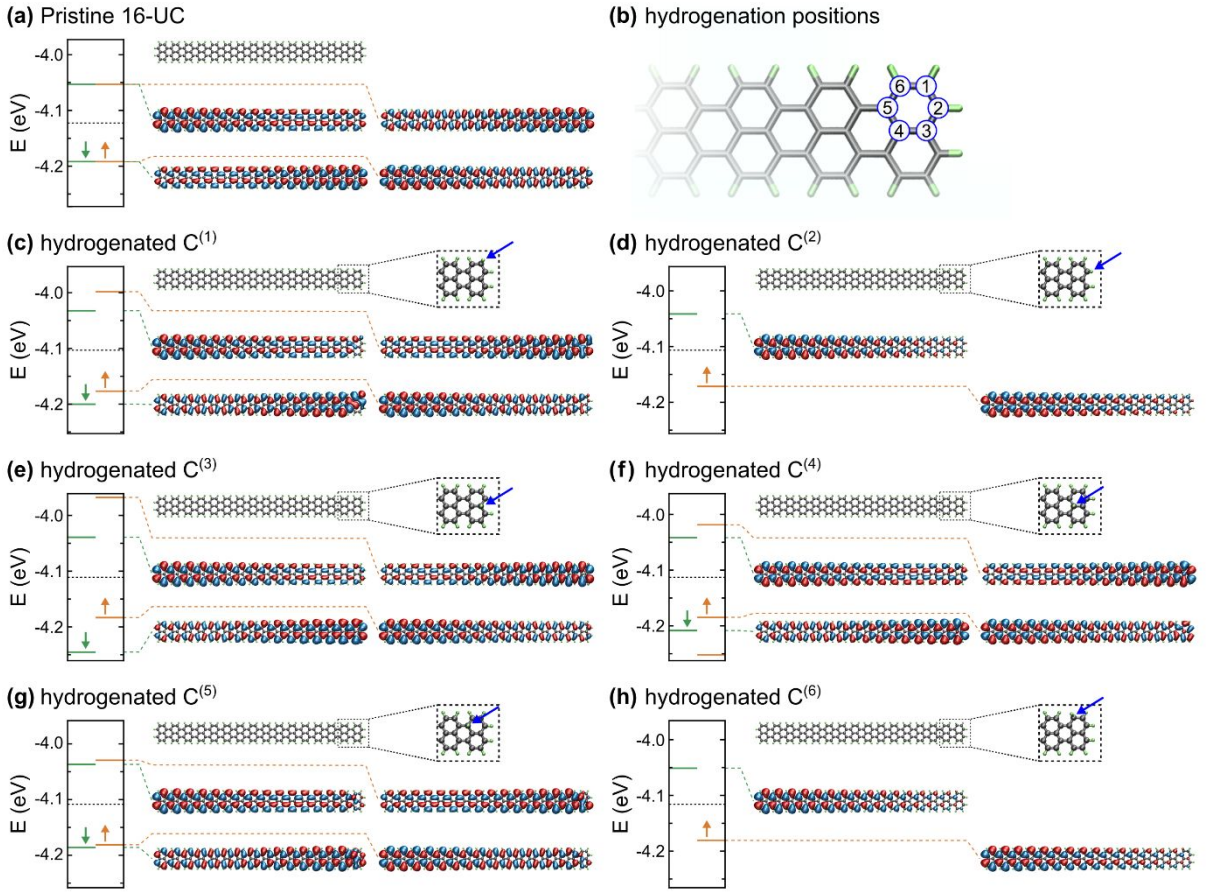

Figure S8. Effect of C atoms hydrogenation on the end states of a 16-UC 5-AGNR. (a) Structure of a pristine 16-UC 5-AGNR and its associated end state orbitals. (b) Different positions of the C atom considered for hydrogenation. (c-h) Structure and associated end state orbitals of a 16-UC 5-GNR with a hydrogenated C atom for each of the positions specified in panel (b). Of all 6 cases considered, only two (labeled as '2' and '6' on panel (b)) resulted in quenching the disturbed end state.

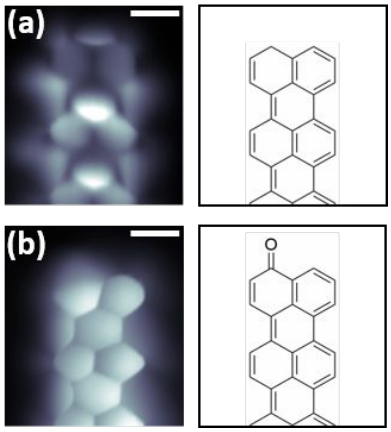

Figure S9. A comparison between constant height HR-STM images of (a) the pristine end of a 5-AGNR (CO tip, 2 mV) and (b) the oxidised end of a 5-AGNR (CO tip, 2 mV). Scale bars are both 3 Å. Due to the presence of the end state at low positive bias voltages, the appearance of the pristine nanoribbons (when above 8 UC in length) was typically a mixture of structural features and the end state. As oxidation destroys the end state, the appearance of oxidised ends is unaffected by this, and the structure is imaged much more clearly.

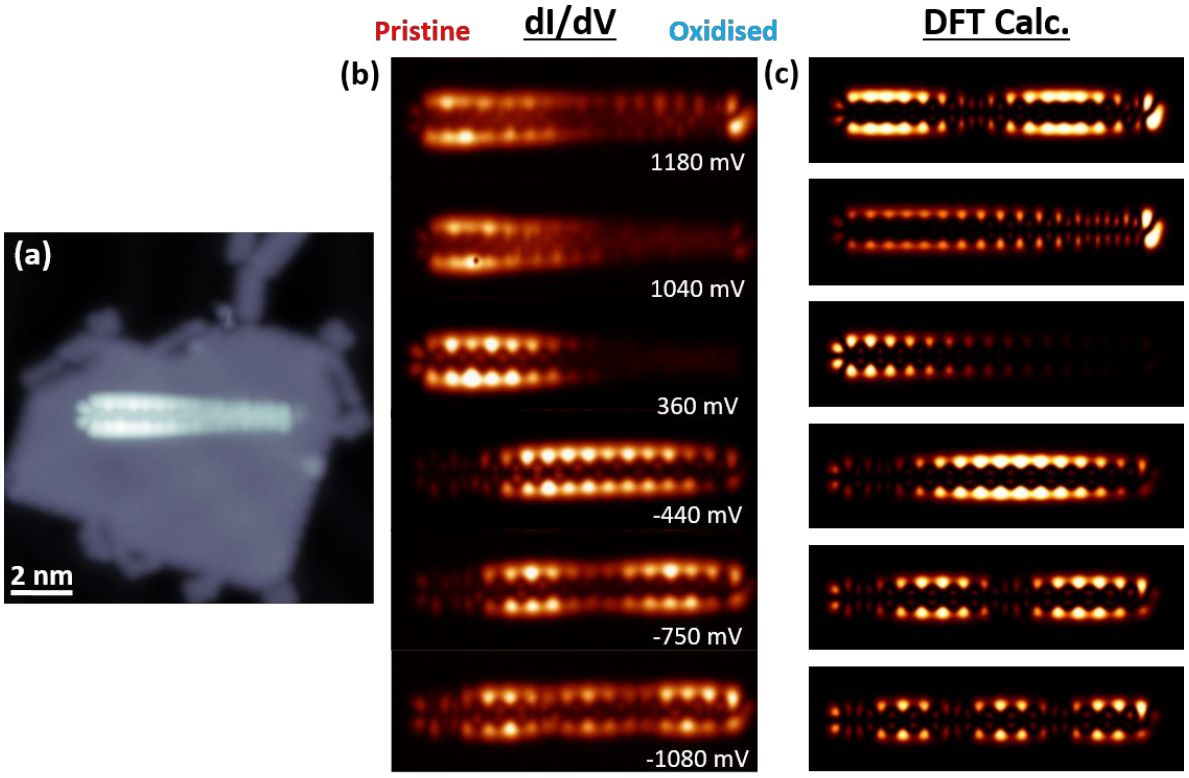

Figure S10. Constant height dI/dV images of the half-oxidised 16-UC nanoribbon shown in the main paper, with the pristine and oxidised ends indicated. In (c), DFT-calculated gas phase molecular orbitals of a half-oxidised 16-UC ribbon are shown. A generally good agreement is found between the

images and the calculations. In particular, the (spatial) shift of the valence band towards the oxidised end is clear in both the experimental results and the calculations, with the opposite effect (*i.e*. a shift towards the pristine end) seen for the conduction band.

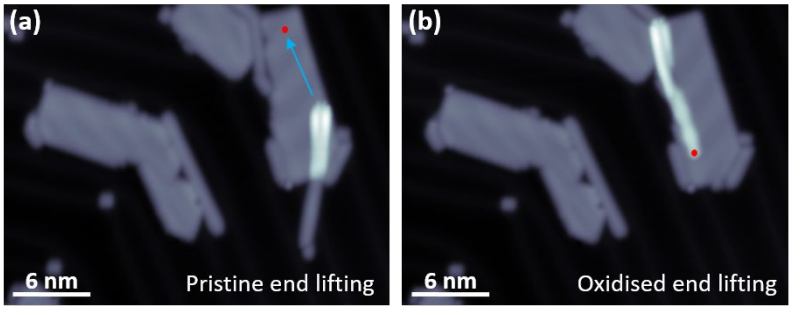

Figure S11. The lifting positions used for the half-oxidised 26-UC data presented in main paper Fig. 7 (c) and (d). (a) The ribbon was first dragged partially onto the NaCl island by its pristine end, and then dragged further in and lifted at the position indicated by its red marker. After this, it was released by a +2V pulse (using the methodology of Wang *et al.*[1]) and landed in the position shown in (b), in which it is decoupled by both the NaCl and also an adjacent nanoribbon. The ribbon was then lifted by its oxidised end, indicated again with a red marker. The exact position of the pristine end of the ribbon during this process is unknown, but it is assumed to be decoupled from the Au substrate due to the magnitude of the current exhibited. Typically when lifting directly from Au(111), the current was found to be of the order of 10^{-7} A when first making contact at 5 mV bias voltage, whereas when lifting on 1 ML NaCl it was generally in the 10^{-9} A range.

Supplementary Methods:

Precursor Synthesis:

The synthesis of the precursors used in this study is described in the supplementary information of the article by Kimouche *et al*.[2], who kindly also allowed us to use their precursors.

References:

(1) Wang, S.; Talirz, L.; Pignedoli, C. A.; Feng, X.; Müllen, K.; Fasel, R.; Ruffieux, P. Giant Edge State Splitting at Atomically Precise Graphene Zigzag Edges. *Nat. Commun.* **2016**, *7*, 11507.

(2) Kimouche, A.; Ervasti, M. M.; Drost, R.; Halonen, S.; Harju, A.; Joensuu, P. M.; Sainio, J.; Liljeroth, P. Ultra-Narrow Metallic Armchair Graphene Nanoribbons. *Nat. Commun.* **2015**, *6*, 10177.